

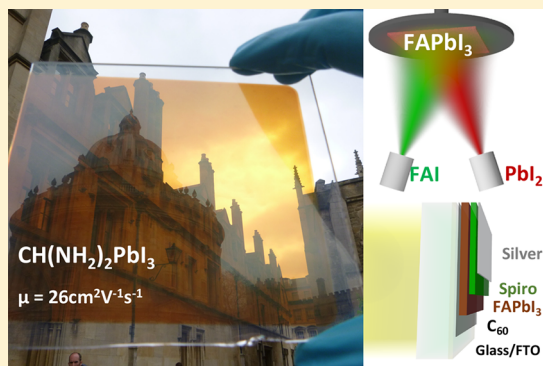
Large-Area, Highly Uniform Evaporated Formamidinium Lead Triiodide Thin Films for Solar Cells

Juliane Borchert, Rebecca L. Milot, Jay B. Patel, Christopher L. Davies, Adam D. Wright, Laura Martínez Maestro, Henry J. Snaith,[†] Laura M. Herz,[‡] and Michael B. Johnston^{*†}

Clarendon Laboratory, Department of Physics, University of Oxford, Parks Road, Oxford OX1 3PU, United Kingdom

Supporting Information

ABSTRACT: Perovskite thin-film solar cells are one of the most promising emerging renewable energy technologies because of their potential for low-cost, large-area fabrication combined with high energy conversion efficiencies. Recently, formamidinium lead triiodide (FAPbI₃) and other formamidinium (CH(NH₂)₂) based perovskites have been explored as interesting alternatives to methylammonium lead triiodide (MAPbI₃) because they exhibit better thermal stability. However, at present a major challenge is the scale-up of perovskite solar cells from small test-cells to full solar modules. We show that coevaporation is a scalable method for the deposition of homogeneous FAPbI₃ thin films over large areas. The method allows precise control over film thickness and results in highly uniform, pinhole-free layers. Our films exhibited a high charge-carrier mobility of 26 cm² V⁻¹s⁻¹, excellent optical properties, and a bimolecular recombination constant of 7 × 10⁻¹¹ cm³ s⁻¹. Solar cells fabricated using these vapor-deposited layers within a regular device architecture produced stabilized power conversion efficiencies of up to 14.2%. Thus, we demonstrate that efficient FAPbI₃ solar cells can be vapor-deposited, which opens up a pathway toward large-area stable perovskite photovoltaics.



Hybrid organic–inorganic perovskite halide solar cells have attracted much attention in recent years because of their remarkably fast rise in power conversion efficiencies (PCE).¹ While PCEs above 20% have been achieved by multiple research groups,^{2–4} the stability and scalability of perovskite solar cells remain obstacles to their commercialization. Methylammonium lead triiodide (CH₃NH₃PbI₃ = MAPbI₃) has been the most commonly used and investigated perovskite solar cell material. However, more recently formamidinium lead triiodide (CH(NH₂)₂PbI₃ = FAPbI₃) and other perovskites containing formamidinium have been studied as they offer a number of advantages over MAPbI₃. Specifically, FAPbI₃ has a narrower band gap of 1.47 eV, which results in an extension of the absorption into the near-infrared,⁵ and FAPbI₃ also exhibits better thermal stability than MAPbI₃.⁶ Mixed-cation perovskites combining formamidinium and other cations such as methylammonium or cesium have been shown to be even more thermally stable,^{7,8} while using both mixed cations and mixed halides enables stable perovskite thin films to be created with a widely tunable band gap.⁹

FAPbI₃ thin films have been fabricated using a variety of methods, with spin-coating from solution being the most

common.^{6,10} Others have used predeposited PbI₂ films which they converted into FAPbI₃ by dipping in solutions containing FAI,⁵ and it has also been demonstrated that FAPbI₃ thin films can be grown in a chemical vapor deposition (CVD) furnace.¹¹

Vacuum-based deposition processes such as coevaporation are advantageous because they result in highly uniform, pinhole-free, smooth thin films.¹² Pinhole-free films are particularly important for large-area solar cells in order to avoid short circuits between electron and hole transport layers that limit PCEs and fill factors. Good thickness uniformity and low roughness are important for reliable solar cell production and also facilitate advanced optoelectronic characterization of the material.¹² Using coevaporation and highly optimized contact layers, efficiencies of up to 20% have been reached for MAPbI₃-based solar cells.³ Additionally, vacuum-based deposition does not require solvents, so it is an ideal method for depositing perovskite thin films in multilayer stacks and on

Received: October 5, 2017

Accepted: November 10, 2017

sensitive substrates. This is particularly useful for the fabrication of tandem solar cells^{8,13} and solar cells on flexible substrates.

In this study, we combine the advantages of formamidinium-based perovskites with the advantages of thermal evaporation under vacuum. We used coevaporation to deposit large-area (8 cm × 8 cm), highly uniform FAPbI₃ thin films that possessed excellent material properties. The films exhibited a high charge-carrier mobility of 26 cm²V⁻¹s⁻¹ and a very low surface roughness with a root-mean-square (R_{RMS}) of only 6.2 nm. We also fabricated efficient solar cell devices based on coevaporated FAPbI₃ which produced PCEs of up to 15.8%, with a stabilized power output (SPO) efficiency of 14.2%.

Solar cells were fabricated using a simple planar architecture on fluoride-doped tin oxide (FTO) coated glass substrates. Briefly, they consisted of an evaporated C₆₀ layer as the electron transport layer,¹⁴ a 300 nm thick absorber layer of coevaporated FAPbI₃, and a spin-coated hole transport layer of 2,2',7,7'-tetrakis(*N,N*-di-4-methoxyphenylamino)-9,9'-spirobifluorene (Spiro-OMeTAD). Finally, multiple 100 nm thick silver electrodes with an area of 9.19 mm² were evaporated; these electrodes defined the pixel size of the test solar cell devices. Full details of device fabrication are provided in the [Supporting Information](#). The device performance was assessed using current density–voltage (J – V) sweeps and photocurrent spectroscopy under simulated sunlight. As shown in [Figure 1a](#), the power conversion efficiency of our champion cell was 15.8% with an open-circuit voltage (V_{OC}) of 1.01 V and a short-circuit current (J_{SC}) of 22.1 mA cm⁻². To test the stabilization of the solar cell performance under working conditions, the same cell was held close to the maximum power point for 50 s. The PCE stabilized at 14.2% ([Figure 1b](#)), and the current stabilized at 17 mA cm⁻².

[Figure 1c](#) shows the external quantum efficiency (EQE) spectrum of the champion device measured in short circuit under 1 sun (1 kW/m² AM1.5) illumination. The EQE peaks at 80% and shows high values over the wavelength range 400–600 nm. However, a drop in EQE to values of ~60% is observed for wavelengths between 600 nm and the FAPbI₃ band-edge. We attribute this feature to optical interference in the planar device-stack, coupled with a lower absorption coefficient of the perovskite layer at longer wavelengths. We therefore anticipate that producing devices with a thicker FAPbI₃ layer and utilizing optical modeling to optimize the thicknesses of all layers in the device stack would further improve the PCE of these cells.

The integrated current over the spectrum is 19 mA cm⁻², which is close to the J_{SC} recorded in the J – V measurements: 22 mA cm⁻² for both the forward and reverse scan, and 17 mA cm⁻² stabilized. Additional cell performance data can be found in the [Supporting Information](#). Overall, we were able to fabricate solar cells with a high PCE which also stabilized at similarly high efficiencies. This result shows that vapor depositing FAPbI₃ yields efficient solar cells in a relatively simple, planar cell architecture.

To assess the uniformity of the coevaporation method, we deposited a large-area (64 cm²) FAPbI₃ film directly onto a glass sheet. Our evaporation system had a relatively short working distance of 20 cm between the thermal sources and the rotating substrate (schematically shown in [Figure 2a](#)). Therefore, it is expected that any evaporated film should be thickest in the center of the substrate, with thickness reducing as a function of radius. A photograph of the deposited film after annealing is shown in [Figure 2b](#). We measured the thickness of the FAPbI₃ layer in three areas on this film using a profilometer.

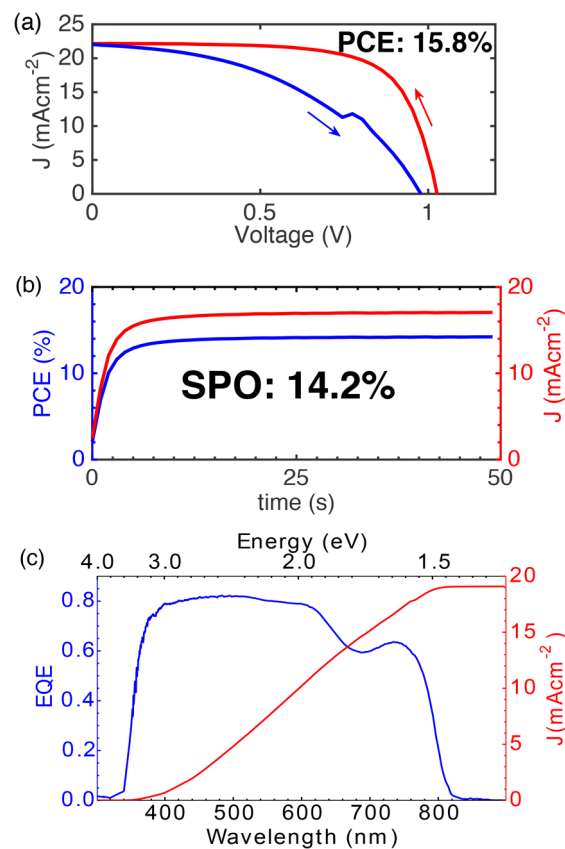


Figure 1. (a) Current–voltage (J – V) curve of the champion evaporated FAPbI₃ device. The short-circuit current density (J_{SC}) was 22.1 mA cm⁻², the open-circuit voltage (V_{OC}) 1.01 V, and the power conversion efficiency (PCE) 15.8%. Significant hysteresis can be observed between the forward (blue) and reverse (red) sweeps. (b) The stabilized power output measurement (SPO), showing a stabilized efficiency of 14.2% (blue) and a stabilized current of 17 mA cm⁻² (red). (c) External quantum efficiency (EQE) spectrum (blue) of the same device with the integrated current over the EQE spectrum (red) being 19 mA cm⁻².

In each area at least seven measurements were performed to calculate a mean thickness value (see [Figure S1](#) for further details). The film had a thickness of 370 ± 20 nm at the center of the substrate, and as expected, the thickness dropped as a function of radius to 330 ± 20 nm in the corners of the substrate. A straightforward approach to further improving the uniformity of the films is to use a deposition system with a large working distance.

We performed atomic force microscopy (AFM) measurements to determine the surface roughness and surface coverage of the film. [Figure 2c](#) is an AFM image recorded over an area of 5 μm × 5 μm. The film is very smooth with a surface roughness of only $R_{\text{RMS}} = 6.2$ nm over the image area. This value is much lower than the surface roughness of FAPbI₃ thin films produced by other methods, with reported roughness values ranging from 18 nm¹⁵ to above 100 nm.¹⁶ We also found that the film was very homogeneous and had no pinholes. We conclude that evaporation leads to significantly smoother and more homogeneous films from which we would expect very little light scattering. Indeed, this is confirmed by the visible absorption, transmission and reflection spectra shown in [Figure 3a](#) where there is very little scatter below the onset of absorption. The absorption onset is around 1.5 eV, which is

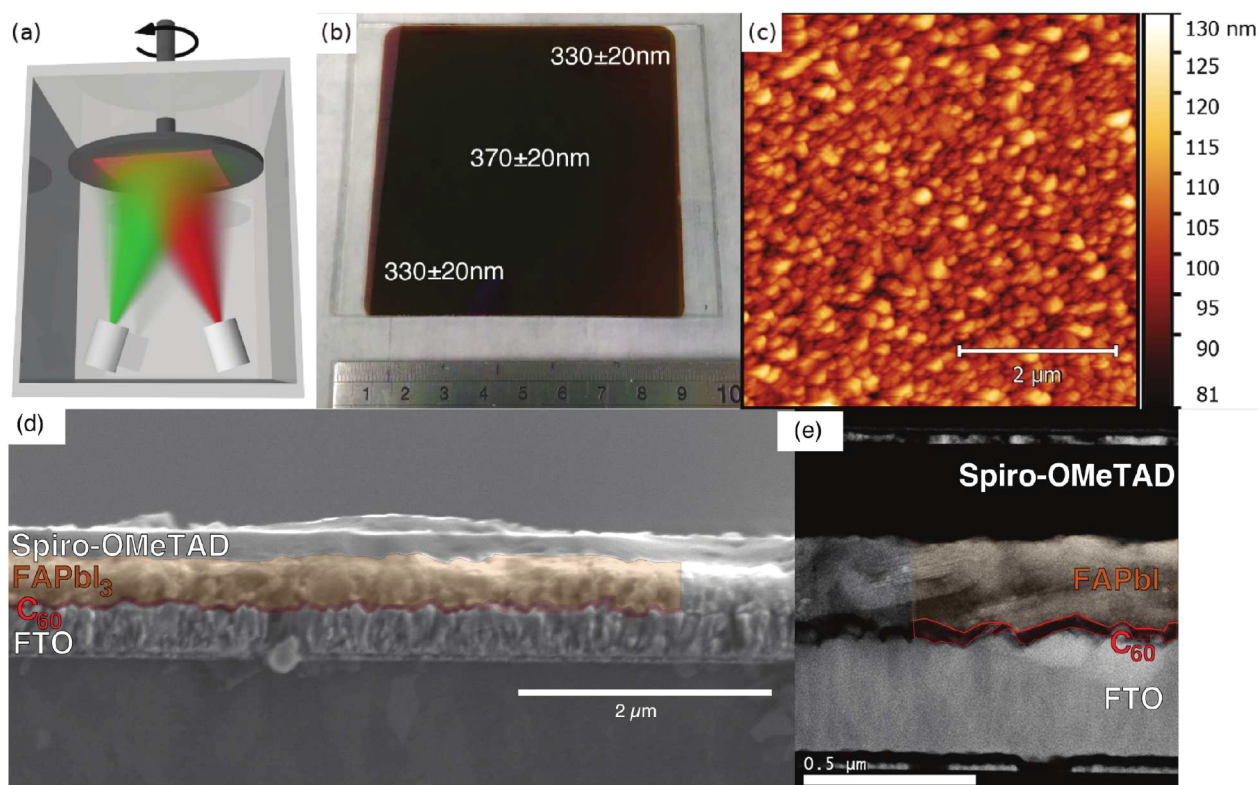


Figure 2. (a) Schematic diagram of the dual-source coevaporation system used in this study. (b) Photograph of 8 cm \times 8 cm thin film of FAPbI₃ deposited on a glass substrate. The image shows the substrate after thermal annealing at 170 °C for 1 min. The results of thickness measurements at three positions are superimposed on the image, and a metal ruler with a centimeter scale is shown as a size reference. (c) Atomic force micrograph of a 5 μ m \times 5 μ m region of the sample. The surface was found to be very smooth with a root-mean-square roughness $R_{\text{RMS}} = 6.2$ nm. (d) A scanning electron microscopy image and (e) a scanning transmission electron microscopy image of a full FAPbI₃ solar cell. From the bottom, the layers are a glass substrate, fluorine doped tin oxide (FTO) layer, thin C₆₀ layer, FAPbI₃ layer, a spiro-OMeTAD layer, and the silver electrode.

consistent with the previously reported values for the absorption onset in solution-processed FAPbI₃. Together, the profilometer, AFM, and absorption measurements show that we fabricated very uniform and smooth FAPbI₃ thin films.

To clarify the crystal phases present in the thin film we performed X-ray diffraction measurements. At room temperature, FAPbI₃ can be either in a black, trigonal, perovskite phase or in a yellow, hexagonal, nonperovskite phase.^{17,18} Only thin films in the black phase are suitable for use as absorbers in solar cells, so it is necessary to ensure that the film is in the right phase. The diffraction patterns are shown in Figure 3b and confirm that after 1 min of annealing at 170 °C the material was in the black perovskite α -FAPbI₃ phase. In the annealed sample, all X-ray reflections are consistent with this α structure; however, in the as-deposited (unannealed) sample, the intensity of the perovskite reflection is strongly reduced, and the most intense peaks are consistent with the yellow, nonperovskite δ phase of FAPbI₃.¹⁷ This confirms that in the as-deposited film the yellow δ -FAPbI₃ is dominant, and upon annealing, it is converted to the black α -FAPbI₃ phase. In evaporated MAPbI₃ thin films, annealing is not necessary to obtain high solar cell efficiencies¹⁹ because there are no competing nonperovskite MAPbI₃ phases. In contrast, for FAPbI₃, annealing is essential in order to obtain the perovskite phase. Overall, we observed the same phase behavior as has been reported for solution-processed FAPbI₃¹⁸ and single crystals.¹⁷ Interestingly for evaporated FAPbI₃ thin films only a very short annealing time is necessary to obtain the desired α -phase. It is well-known that

the α -FAPbI₃ phase is not long-term stable and converts to a yellow hexagonal phase when exposed to humidity (see Figure S5). To address this problem, coevaporation of cesium, methylammonium, or bromide could be used to stabilize the perovskite phase.

To learn more about the morphology of the films and the crystal quality, we performed scanning electron microscopy (SEM) and scanning transmission electron microscopy (STEM) on full solar cell devices. A typical cross-sectional SEM image of a device is shown in Figure 2d where a smooth, uniform film of FAPbI₃ (colored brown in the image) can be seen. In our survey of cross sections we did not observe any evidence of pinholes in the FAPbI₃ layer. To observe the crystal quality and interfaces, high-resolution STEM images were taken on thin cross-sectional lamella of the device. The lamella were prepared using a focused ion beam (FIB), as described in the Supporting Information. The STEM image in Figure 2e shows crystallites of different orientations within the perovskite film, with some extending vertically through the film. The STEM image also shows high contrast between the FAPbI₃ (bright) and the carbon-rich (dark) C₆₀ and Spiro-OMeTAD that surround it. Close inspection of Figure 2e reveals regions of direct contact between the FAPbI₃ and FTO layers which have been shown previously to lead to hysteretic J - V curves similar to that shown in Figure 1a.¹⁹

The photoluminescence (PL) spectrum of a coevaporated and annealed FAPbI₃ film is shown in the inset of Figure 4a. The PL peak is at a wavelength of approximately 805 nm (1.54

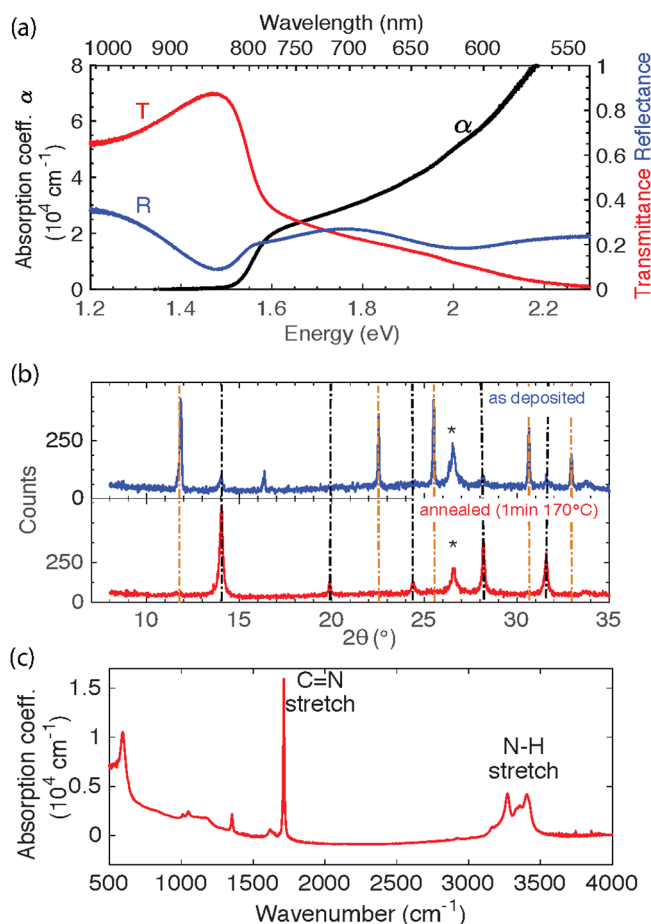


Figure 3. (a) Absorption (black line) of the coevaporated FAPbI₃ thin films in the visible is calculated from the transmission (red line) and reflection (blue line) spectra. As expected, an absorption onset around 1.5 eV is observed. (b) X-ray diffraction pattern for an as-deposited and for an annealed film. The orange lines mark the expected position corresponding to the yellow nonperovskite δ -FAPbI₃ phase, whereas the black dashed lines mark the peaks matching the perovskite α -FAPbI₃ phase.¹⁷ The star marks the FTO substrate peak. (c) Infrared absorption spectrum of the film showing the characteristic absorption peaks for FAPbI₃.

eV) in agreement with previous reports for solution-processed FAPbI₃.^{6,17,20} The full width at half-maximum of the PL spectrum for the vapor-deposited sample was 79 meV, which is slightly narrower than that previously reported for a solution-processed sample (88 meV).²⁰ Because PL broadening is a combination of both homogeneous broadening and disorder broadening,²¹ the narrower PL emission observed from the evaporated films may be an indication of reduced disorder; however, an in-depth study of PL as a function of excitation fluence and temperature would be required to confirm this. **Figure 4a** shows the measured time-resolved PL transient fitted with a stretched exponential function in order to account for a superposition of exponential decays.^{19,22} The average monomolecular lifetime, τ , of these decays is 2 ns, which is significantly lower than that typically reported for solution-processed FAPbI₃ films.^{6,23,24} Our measured lifetimes are similar to previously reported lifetimes for vapor-deposited MAPbI₃ films.²⁵ Optimization of deposition parameters to increase the PL lifetime offers another opportunity to improve the efficiency of solar cells based on these films, which show remarkably high PCEs given the very short PL lifetimes.

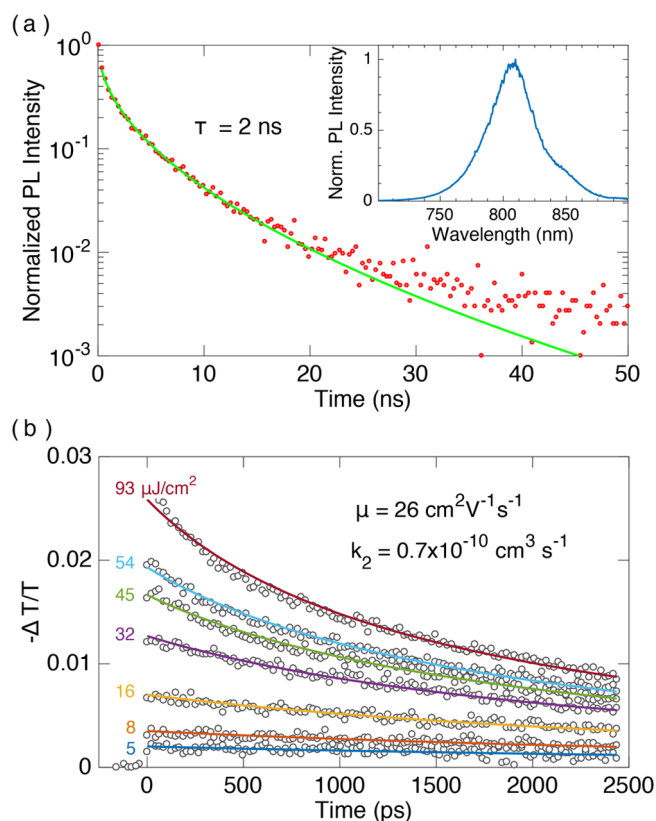


Figure 4. (a) Photoluminescence (PL) from an evaporated FAPbI₃ thin film. The PL decay is fit using a stretched exponential function to extract an average monomolecular charge-carrier lifetime of 2 ns. The PL spectrum shown in the inset has a peak at 805 nm (1.54 eV). (b) Optical pump/THz probe measurements of the charge-carrier recombination dynamics in the evaporated FAPbI₃ thin film on z-cut quartz. The sample was photoexcited at 400 nm with various fluences ranging from 5 to 93 $\mu\text{J}/\text{cm}^2$ as labeled on the graph. The open circles represent experimental data points, and the solid lines are fits to eq 1 of the [Supporting Information](#).

Terahertz (THz) photoconductivity measurements were performed to assess the charge mobility and recombination dynamics in coevaporated FAPbI₃. **Figure 4b** shows the change in photoconductivity for a thin film of coevaporated FAPbI₃ as a function of time after photoexcitation with 35 fs laser pulses. From these data the charge-carrier mobility was found to be 26 $\text{cm}^2 \text{V}^{-1} \text{s}^{-1}$, and an apparent²⁶ bimolecular recombination rate constant of $k_2^{\text{apparent}} = 0.7 \times 10^{-10} \text{cm}^3 \text{s}^{-1}$ was extracted. Both parameters are nearly identical to the values determined for solution-processed FAPbI₃ films.^{24,27} Using the measured carrier lifetime and mobility we extract a charge-carrier diffusion length²⁴ of 360 nm for a charge carrier density typical for this material under solar illumination (10^{15}cm^{-3}).²⁷ This is longer than the thickness of our absorber layer and therefore sufficiently long to allow the charges to migrate to the interfaces with the charge transport layers. These THz measurements show that the evaporated FAPbI₃ possesses good charge conduction properties, comparable with the perovskite materials used in high-efficiency solar cells.

We were able to coevaporate formamidinium iodide and lead iodide to deposit FAPbI₃ thin films. The deposited films were smooth and uniform over a large area of roughly $8 \times 8 \text{cm}^2$, which demonstrates the advantages of vapor deposition for large-area perovskite solar cells. The film properties were

similar to previously reported properties of FAPbI₃. We fabricated solar cells from these thin films and achieved a stabilized power conversion efficiency of 14.2%. This is a highly promising result which with further improvements in interface engineering can lead to even higher efficiencies. Being able to vapor deposit FAPbI₃ is a key step towards the scale-up of perovskite solar cells.²⁸ It opens up the possibility of fabricating the more stable, multication perovskites such as FA_yCs_{y-1}Pb_{1-x}(I_{1-x}Br_x)₃ using the highly scalable coevaporation route. Thus, our results are an important milestone on the way to large-area, stable thin-film perovskite solar cells.

■ ASSOCIATED CONTENT

● Supporting Information

The Supporting Information is available free of charge on the ACS Publications website at DOI: [10.1021/acsenergylett.7b00967](https://doi.org/10.1021/acsenergylett.7b00967).

Additional experimental procedures and characterization data such as scanning electron microscopy images, additional atomic force microscopy images, photos illustrating the phase transition to the yellow phase, and additional data about the spread of solar cell performance (PDF)

■ AUTHOR INFORMATION

Corresponding Author

*E-mail: michael.johnston@physics.ox.ac.uk.

ORCID

Henry J. Snaith: 0000-0001-8511-790X

Laura M. Herz: 0000-0001-9621-334X

Michael B. Johnston: 0000-0002-0301-8033

Notes

The authors declare no competing financial interest.

■ ACKNOWLEDGMENTS

The authors gratefully acknowledge the financial support from the Engineering and Physical Sciences Research Council (U.K.) (EPSRC). J.B.P. thanks the EPSRC and Merck Chemicals for the financial support through an Industrial CASE studentship. J.B. thanks the EPSRC for funding via the Centre for Doctoral Training in New and Sustainable Photovoltaics. A.D.W. thanks the EPSRC for funding via the Centre for Doctoral Training in Plastic Electronics.

■ REFERENCES

- (1) Correa-Baena, J.-P.; Abate, A.; Saliba, M.; Tress, W.; Jacobsson, T. J.; Grätzel, M.; Hagfeldt, A. The rapid evolution of highly efficient perovskite solar cells. *Energy Environ. Sci.* **2017**, *10*, 710–727.
- (2) Yang, W. S.; Park, B.-W.; Jung, E. H.; Jeon, N. J.; Kim, Y. C.; Lee, D. U.; Shin, S. S.; Seo, J.; Kim, E. K.; Noh, J. H.; Seok, S. I. Iodide management in formamidinium-lead-halide-based perovskite layers for efficient solar cells. *Science* **2017**, *356*, 1376–1379.
- (3) Momblona, C.; Gil-Escrig, L. N.; Bandiello, E.; Hutter, E. M.; Sessolo, M.; Lederer, K.; Blochwitz-Nimoth, J.; Bolink, H. J. Efficient vacuum deposited p-i-n and n-i-p perovskite solar cells employing doped charge transport layers. *Energy Environ. Sci.* **2016**, *9*, 3456–3463.
- (4) Saliba, M.; Matsui, T.; Seo, J.-Y.; Domanski, K.; Correa-Baena, J.-P.; Nazeeruddin, M. K.; Zakeeruddin, S. M.; Tress, W.; Abate, A.; Hagfeldt, A.; et al. Cesium-containing triple cation perovskite solar cells: improved stability, reproducibility and high efficiency. *Energy Environ. Sci.* **2016**, *9*, 1989–1997.
- (5) Koh, T. M.; Fu, K.; Fang, Y.; Chen, S.; Sum, T. C.; Mathews, N.; Mhaisalkar, S. G.; Boix, P. P.; Baikie, T. Formamidinium-containing metal-halide: An alternative material for near-IR absorption perovskite solar cells. *J. Phys. Chem. C* **2014**, *118*, 16458–16462.
- (6) Eperon, G. E.; Stranks, S. D.; Menelaou, C.; Johnston, M. B.; Herz, L. M.; Snaith, H. J. Formamidinium lead trihalide: a broadly tunable perovskite for efficient planar heterojunction solar cells. *Energy Environ. Sci.* **2014**, *7*, 982–988.
- (7) Habisreutinger, S. N.; McMeekin, D. P.; Snaith, H. J.; Nicholas, R. J. Research Update: Strategies for improving the stability of perovskite solar cells. *APL Mater.* **2016**, *4*, 091503.
- (8) McMeekin, D. P.; Sadoughi, G.; Rehman, W.; Eperon, G. E.; Saliba, M.; Hörantner, M. T.; Haghighirad, A.; Sakai, N.; Korte, L.; Rech, B.; et al. A mixed-cation lead mixed-halide perovskite absorber for tandem solar cells. *Science* **2016**, *351*, 151–155.
- (9) Wang, Z.; McMeekin, D. P.; Sakai, N.; van Reenen, S.; Wojciechowski, K.; Patel, J. B.; Johnston, M. B.; Snaith, H. J. Efficient and air-stable mixed-cation lead mixed-halide perovskite solar cells with n-doped organic electron extraction layers. *Adv. Mater.* **2017**, *29*, 1604186.
- (10) Lv, S.; Pang, S.; Zhou, Y.; Padture, N. P.; Hu, H.; Wang, L.; Zhou, X.; Zhu, H.; Zhang, L.; Huang, C.; et al. One-step solution-processed formamidinium lead trihalide (FAPbI_(3-x)Cl_x) for mesoscopic perovskite-polymer solar cells. *Phys. Chem. Chem. Phys.* **2014**, *16*, 19206.
- (11) Leyden, M. R.; Jiang, Y.; Qi, Y. Chemical vapor deposition grown formamidinium perovskite solar modules with high steady state power and thermal stability. *J. Mater. Chem. A* **2016**, *4*, 13125–13132.
- (12) Liu, M.; Johnston, M. B.; Snaith, H. J. Efficient planar heterojunction perovskite solar cells by vapour deposition. *Nature* **2013**, *501*, 395–398.
- (13) Eperon, G. E.; Leijtens, T.; Bush, K. A.; Prasanna, R.; Green, T.; Wang, J. T.-W.; McMeekin, D. P.; Volonakis, G.; Milot, R. L.; May, R.; et al. Perovskite-perovskite tandem photovoltaics with optimized band gaps. *Science (Washington, DC, U. S.)* **2016**, *354*, 861–865.
- (14) Zhao, D.; Ke, W.; Grice, C. R.; Cimaroli, A. J.; Tan, X.; Yang, M.; Collins, R. W.; Zhang, H.; Zhu, K.; Yan, Y. Annealing-free efficient vacuum-deposited planar perovskite solar cells with evaporated fullerenes as electron-selective layers. *Nano Energy* **2016**, *19*, 88–97.
- (15) Yu, Y.; Wang, C.; Grice, C. R.; Shrestha, N.; Chen, J.; Zhao, D.; Liao, W.; Cimaroli, A. J.; Roland, P. J.; Ellingson, R. J.; et al. Improving the performance of formamidinium and cesium lead triiodide perovskite solar cells using lead thiocyanate additives. *ChemSusChem* **2016**, *9*, 3288–3297.
- (16) Xie, Z.; Sun, S.; Yan, Y.; Zhang, L.; Hou, R.; Tian, F.; Qin, G. G. Refractive index and extinction coefficient of NH₂CH = NH₂PbI₃ perovskite photovoltaic material. *J. Phys.: Condens. Matter* **2017**, *29*, 245702.
- (17) Stoumpos, C. C.; Malliakas, C. D.; Kanatzidis, M. G. Semiconducting tin and lead iodide perovskites with organic cations: Phase transitions, high mobilities, and near-infrared photoluminescent properties. *Inorg. Chem.* **2013**, *52*, 9019–9038.
- (18) Binek, A.; Hanusch, F. C.; Docampo, P.; Bein, T. Stabilization of the trigonal high-temperature phase of formamidinium lead iodide. *J. Phys. Chem. Lett.* **2015**, *6*, 1249–1253.
- (19) Patel, J. B.; Wong-Leung, J.; Van Reenen, S.; Sakai, N.; Wang, J. T. W.; Parrott, E. S.; Liu, M.; Snaith, H. J.; Herz, L. M.; Johnston, M. B. Influence of interface morphology on hysteresis in vapor-deposited perovskite solar cells. *Adv. Electron. Mater.* **2017**, *3*, 1600470.
- (20) Wright, A. D.; Verdi, C.; Milot, R. L.; Eperon, G. E.; Pérez-Osorio, M. A.; Snaith, H. J.; Giustino, F.; Johnston, M. B.; Herz, L. M. Electron-phonon coupling in hybrid lead halide perovskites. *Nat. Commun.* **2016**, *7*, 11755.
- (21) Wright, A. D.; Milot, R. L.; Eperon, G. E.; Snaith, H. J.; Johnston, M. B.; Herz, L. M. Band-Tail Recombination in Hybrid Lead Iodide Perovskite. *Adv. Funct. Mater.* **2017**, *27*, 1700860.
- (22) de Quilettes, D. W.; Vorpahl, S. M.; Stranks, S. D.; Nagaoka, H.; Eperon, G. E.; Ziffer, M. E.; Snaith, H. J.; Ginger, D. S. Impact of

microstructure on local carrier lifetime in perovskite solar cells. *Science* **2015**, *348*, 683–686.

(23) Pellet, N.; Gao, P.; Gregori, G.; Yang, T.-Y.; Nazeeruddin, M. K.; Maier, J.; Grätzel, M. Mixed-organic-cation perovskite photovoltaics for enhanced solar-light harvesting. *Angew. Chem., Int. Ed.* **2014**, *53*, 3151–7.

(24) Rehman, W.; Milot, R. L.; Eperon, G. E.; Wehrenfennig, C.; Boland, J. L.; Snaith, H. J.; Johnston, M. B.; Herz, L. M. Charge-carrier dynamics and mobilities in formamidinium lead mixed-halide perovskites. *Adv. Mater.* **2015**, *27*, 7938–7944.

(25) Patel, J. B.; Milot, R. L.; Wright, A. D.; Herz, L. M.; Johnston, M. B. Formation dynamics of $\text{CH}_3\text{NH}_3\text{PbI}_3$ perovskite following two-step layer deposition. *J. Phys. Chem. Lett.* **2016**, *7*, 96–102.

(26) Crothers, T. W.; Milot, R. L.; Patel, J. B.; Parrott, E. S.; Schlipf, J.; Müller-Buschbaum, P.; Johnston, M. B.; Herz, L. M. Photon reabsorption masks intrinsic bimolecular charge-carrier recombination in $\text{CH}_3\text{NH}_3\text{PbI}_3$ perovskite. *Nano Lett.* **2017**, *17*, 5782–5789. PMID: 28792767.

(27) Johnston, M. B.; Herz, L. M. Hybrid perovskites for photovoltaics: Charge-carrier recombination, diffusion, and radiative efficiencies. *Acc. Chem. Res.* **2016**, *49*, 146–154.

(28) Sessolo, M.; Momblona, C.; Gil-Escrig, L.; Bolink, H. J. Photovoltaic devices employing vacuum-deposited perovskite layers. *MRS Bull.* **2015**, *40*, 660–666.